Contribution from the Department of Chemistry,
University of Minnesota, Minneapolis, Minnesota 55455

Axial vs Equatorial Substitution of $Os_3(CO)_{12}$ with Anionic Ligands. Crystal and Molecular Structures of $PPN[Os_3X(CO)_{11}]$ (X = Br, I)

Janet L. Zuffa, Steven J. Kivi, and Wayne L. Gladfelter*

Received September 14, 1988

The reactions of bis(triphenylphosphine)nitrogen(1+) (PPN) salts of chloride, bromide, and iodide with $Os_3(CO)_{12}$ in the presence of trimethylamine *N*-oxide give the monoanionic clusters $PPN[Os_3X(CO)_{11}]$, where X = Cl, Br, and I, respectively. $PPN(N_3)$ reacts directly with $Os_3(CO)_{12}$ to give the isocyanato-containing cluster $PPN[Os_3(NCO)(CO)_{11}]$. Single-crystal X-ray crystallographic analyses of $PPN[Os_3Br(CO)_{11}]$ [$P2_1/c$ space group, a = 14.191 (32) Å, b = 17.986 (12) Å, c = 18.160 (7) Å, β = 90.36 (10)°, Z = 4] and $PPN[Os_3I(CO)_{11}]$ [$P2_1/c$ space group, a = 14.696 (14) Å, b = 19.584 (14) Å, c = 16.604 (11) Å, β = 95.17 (7)°, Z = 4] revealed that the basic Os_3L_{12} structure is preserved. The bromide was located in an axial position, whereas the iodide is coordinated in the equatorial plane. ^{13}C NMR spectroscopy at low temperature revealed that the solid-state structures of $[Os_3Br(CO)_{11}]^-$ and $[Os_3I(CO)_{11}]^-$ are maintained in solution and that in both $[Os_3(NCO)(CO)_{11}]^-$ and $[Os_3Cl(CO)_{11}]^-$ the anionic ligand resides in an axial position. The lowest temperature fluxional process for X = Cl, Br, and NCO involved complete exchange of all the equatorial carbonyls. This was followed at higher temperatures by a series of trigonal twists and/or pairwise bridge-terminal CO-exchange steps that allowed all carbonyls to exchange with one another. In the iodo cluster, all carbonyl resonances were found to uniformly broaden and coalesce into one average resonance. It is proposed that this occurs when a rate-determining trigonal twist of the $OsI(CO)_2$ group moves the iodide out of the equatorial plane.

Introduction

We recently reported[1] that coordination of one isocyanate ligand to $Ru_3(CO)_{12}$ converts the completely inactive cluster into one that is among the most active metal carbonyl based hydrogenation catalysts regardless of nuclearity. This has focused our attention on understanding the basic interaction of halides and pseudohalides with metal carbonyls.[2] Other recent developments in the area of activation of metal carbonyl clusters have involved the use of anionic ligands to labilize carbonyl ligands. The discovery by Lavigne and Kaesz[3] that substitution of CO with phosphines on $Ru_3(CO)_{12}$ is effectively catalyzed by halides and pseudohalides was complemented by reports from Ford and co-workers[4] and Darensbourg and co-workers[5] that methoxide catalyzed CO substitutions. Hydride donors also have been utilized to catalyze the substitution of CO on $Ru_3(CO)_{12}$.[6] Many basic questions remain unanswered regarding the effect that the anion has on the metal cluster. Does the anion cause a systematic weakening of selected M-CO bonds? Does the activation occur by a stabilization of the transition state of the substitution reaction as the studies of mononuclear complexes such as $MnBr(CO)_5$ indicate?[7]

The answer to the first question must be evaluated by a comparison of structural studies of halo carbonyl clusters. Few studies are available on the trinuclear clusters having the general formula $[M_3X_n(CO)_m]^{n-}$. The need to focus initially on these simpler systems is 2-fold. First, the formulas differ from the well-known binary metal carbonyls by one type of ligand, and second, the reactivity of these compounds are most greatly altered by the presence of the anion. In this paper we will describe the synthesis and solid-state and solution structures of the family of anionic osmium clusters $[Os_3X(CO)_{11}]^-$. The results show an interesting dependence of the site of substitution on the size of the anion.

Experimental Section

$Os_3(CO)_{12}$[8] and PPN(X) (X = Cl,[9] Br,[10] I,[10] N_3[10]) (PPN = bis(triphenylphosphine)nitrogen(1+) cation) were prepared according to literature procedures. Trimethylamine *N*-oxide dihydrate was purchased from Aldrich and sublimed prior to use. Tetrahydrofuran (THF) and diethyl ether (Et_2O) were distilled under N_2 from sodium benzophenone ketyl. Hexane was dried by distillation from sodium metal under N_2. Hydrogen (H_2) was purchased from Air Products, and ^{13}CO (99%) was purchased from ICN Biomedicals. Both were used without further purification. All reactions were carried out under an atmosphere of N_2 by using standard Schlenk techniques unless otherwise noted. Infrared spectra were recorded on a Mattson Cygnus 25 FTIR spectrophotometer equipped with a HgCdTe detector. NMR spectra were recorded on a Nicolet NTCFT-1130 300 MHz spectrometer in $CDCl_3$ or CD_2Cl_2. Constant temperature was maintained in the probe by using a TRI Research T-2000 Cryo Controller and was calibrated by using a sample of HCl in methanol. $Os_3(CO)_{12}$ was enriched to ca. 30% by heating under 1 atm ^{13}CO at 120 °C for 4 days. ^{13}CO-enriched anions were prepared from enriched $Os_3(CO)_{12}$. Elemental analyses were performed by Galbraith Laboratories or M-H-W Laboratories.

Synthesis of $PPN[Os_3(X)(CO)_{11}]$ (X = Cl, Br, I). $Os_3(CO)_{12}$ (30 mg, 0.03 mmol), Me_3NO (4 mg, 1.5 equiv), and 1 equiv of the appropriate PPN(X) salt were placed into a Schlenk tube equipped with a stir bar. Dry THF (8 mL) was added via syringe, and the solution was stirred under N_2 for 2 h and was filtered. The solvent was removed under vacuum, and a small amount of Et_2O was added. The products precipitated from Et_2O as microcrystals, which were filtered in air and washed with hexane.

X = Cl. Yield: 56% as yellow-orange microcrystals. Anal. Calcd for $C_{47}H_{30}ClNO_{11}Os_3P_2$: C, 38.86; H, 2.08; Cl, 2.44. Found: C, 38.74; H, 2.36; Cl, 2.63. IR (THF): ν_{CO} 2098 w, 2063 w, 2044 m, 2031 m, 2006 s, 1987 m, 1966 m (sh), 1959 m, 1935 w cm^{-1}. ^{13}C NMR [CD_2Cl_2, -85 °C, ppm (relative intensity)]: 189.0 (2), 186.1 (2), 184.9 (1), 182-177 (exchange broadened).

X = Br. Yield: 75% as yellow-orange microcrystals. Anal. Calcd for $C_{47}H_{30}BrNO_{11}Os_3P_2$: C, 37.69; H, 2.02; Br, 5.34. Found: C, 37.42; H, 2.01; Br, 5.56. IR (THF): ν_{CO} 2098 w, 2070 w, 2043 m, 2031 m, 2005 s, 1987 m, 1967 m (sh), 1960 m 1932 w cm^{-1}. ^{13}C NMR [CD_2Cl_2, -89 °C, ppm (relative intensity)]: 188.0 (2), 185.4 (2), 183.9 (1), 181 (exchange broadened), 178 (exchange broadened), 176 (exchange broadened).

X = I. Yield: 84% as red-orange microcrystals. Anal. Calcd for $C_{47}H_{30}INO_{11}Os_3P_2$: C, 36.56; H, 1.96; I, 8.23. Found: C, 36.24; H, 1.89; I, 8.71. IR (THF): ν_{CO} 2096 w, 2084 vw (sh), 2038 m, 2021 m, 2003 s, 1978 m(sh), 1973 m, 1959 m, 1932 w cm^{-1}. ^{13}C NMR [CD_2Cl_2, -90 °C, ppm (relative intensity)]: 193.1 (2), 189.1 (2), 184.4 (2), 181.5 (1), 177.1 (1), 173.5 (2), 170.8 (1).

Synthesis of $PPN[Os_3(NCO)(CO)_{11}]$. $PPN(N_3)$ (134.7 mg, 0.23 mmol) and $Os_3(CO)_{12}$ (210.3 mg, 0.23 mmol) were placed into a Schlenk tube equipped with a stir bar. The flask was evacuated and filled with N_2 three times. THF (20 mL) was added via syringe, and the solution was allowed to stir under N_2 until all the $PPN(N_3)$ had dissolved (15 min). The solvent was removed under vacuum, and Et_2O (10 mL) was added. The product precipitated from Et_2O as slightly air-sensitive golden microcrystals, which were filtered in air and washed with hexane to yield 306 mg (90% yield) of product. Anal. Calcd for $C_{48}H_{30}N_2O_{12}Os_3P_2$: C, 39.51; H, 2.07; N, 1.85. Found: C, 39.08; H, 2.08; N, 1.87. IR (THF): ν_{NCO} 2248 m (br) cm^{-1}; ν_{CO} 2098 w, 2068 w, 2043 m, 2031 m, 2006 s, 1994 m (sh), 1984 m (sh), 1970 m (sh), 1961

(1) Zuffa, J. L.; Blohm, M. L.; Gladfelter, W. L. *J. Am. Chem. Soc.* **1986**, *108*, 552.
(2) Zuffa, J. L.; Gladfelter, W. L. *J. Am. Chem. Soc.* **1986**, *108*, 4669.
(3) Lavigne, G.; Kaesz, H. D. *J. Am. Chem. Soc.* **1984**, *106*, 4647.
(4) Anstock, M.; Taube, D.; Gross, D. C.; Ford, P. C. *J. Am. Chem. Soc.* **1984**, *106*, 3696.
(5) Darensbourg, D. J.; Gray, R. L.; Pala, M. *Organometallics* **1984**, *3*, 1928.
(6) Lavigne, G.; Lugan, N.; Bonnet, J.-J. *Inorg. Chem.* **1987**, *26*, 2345.
(7) Atwood, J. D.; Brown, T. L. *J. Am. Chem. Soc.* **1975**, *97*, 3380-3385.
(8) Johnson, B. F. G.; Lewis, J.; Kilty, P. A. *J. Chem. Soc. A* **1968**, 2859.
(9) Ruff, J. K.; Schlentz, W. J. *Inorg. Synth.* **1974**, *15*, 85-87.
(10) Martinsen, A.; Songstad, J. *Acta Chem. Scand., Ser. A* **1977**, *A31*, 645.

0020-1669/89/1328-1888$01.50/0

Table I. Summary of Crystallographic Data

compd	$PPN[Os_3Br(CO)_{11}]$	$PPN[Os_3I(CO)_{11}]$
formula	$C_{47}H_{30}BrNO_{11}Os_3P_2$	$C_{47}H_{30}INO_{11}Os_3P_2$
fw	1497.22	1544.22
space group	$P2_1/c$	$P2_1/c$
a, Å	14.191 (32)	14.696 (14)
b, Å	17.986 (12)	19.584 (14)
c, Å	18.160 (7)	16.604 (11)
β, deg	90.36 (10)	95.17 (7)
V, Å^3	4635 (15)	4759 (12)
Z	4	4
ρ(calcd), g cm^{-3}	2.145	2.155
temp, °C	−93	−88
μ, cm^{-1}	91.97	87.68
max to min trans factors, %	99.8–78.4	99.8–58.7
R	0.057	0.062
R_w	0.053	0.057

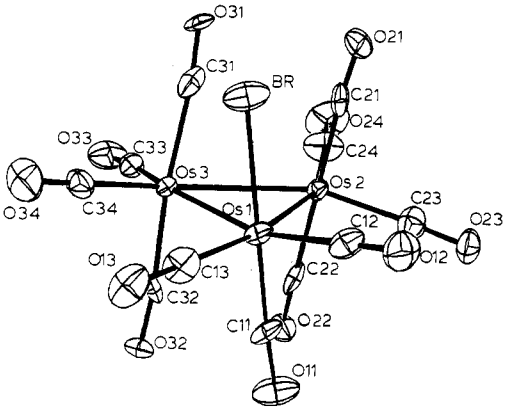

Figure 1. Structure of the anion in $PPN[Os_3Br(CO)_{11}]$, using 50% probability ellipsoids.

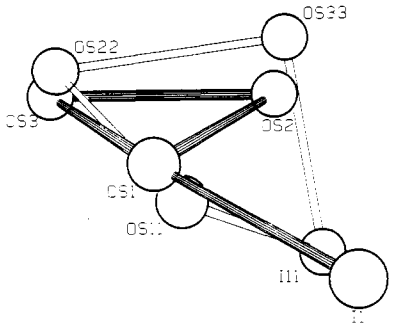

Figure 2. The major and minor orientations of the Os_3I fragment.

m, 1938 w cm^{-1}. ^{13}C NMR [CD_2Cl_2, −84 °C, ppm (relative intensity)]: 187.5 (2), 185.6 (2), 183.3 (1), 179.4 (2), 178.1 (2), 176.6 (2).

X-ray Crystallographic Studies. Details of the structural analyses for both compounds are listed in Table I. Additional details are included in previous structural studies of related compounds examined in our laboratory. The values of the atomic scattering factors used in the calculations were taken from the usual tabulation,[11] and the effects of anomalous dispersion were included for the non-hydrogen atoms.

$PPN[Os_3Br(CO)_{11}]$. Transparent orange prisms of the compound were grown from solutions of THF/ether. The crystal was mounted on a glass fiber and coated with STP to protect it from the atmosphere. The crystal was cooled in a stream of cold nitrogen to −93 °C. A preliminary peak search indicated the crystal was monoclinic, and the systematic absences were consistent only with the space group $P2_1/c$. During the data collection three check reflections indicated a 3.9% decay of intensity. A linear correction was applied to all of the data.

The large number of variables required that the anion and cation be refined in separate least-squares cycles. After convergence the hydrogen atoms were added to the list (but not refined) in their idealized positions with a fixed isotropic thermal parameter of 3.5. The final difference Fourier map revealed nine peaks greater than 1 e/Å^3; five of these (including the two most intense) were located near the Os atoms. The positional parameters, bond distances, and bond angles are listed in Tables II–IV, and Figure 1 illustrates the structure of the anion.

$PPN[Os_3I(CO)_{11}]$. Orange crystals were obtained from THF/ether solutions and mounted on a glass fiber. The crystal was cooled in a stream of cold nitrogen to −88 °C. A preliminary peak search indicated the crystal was monoclinic, and the systematic absences were consistent only with the space group $P2_1/c$. During the data collection three check reflections indicated a 4.9% decay of intensity. A linear correction was applied to all of the data.

(11) (a) Cromer, D. T.; Waber, J. T. *International Tables for X-ray Crystallography*; Kynoch Press: Birmingham, England, 1974; Vol. IV, Table 2.2A. Cromer, D. T. *Ibid.*, Table 2.3.1. (b) Cromer, D. T.; Ibers, J. A. *International Tables of X-ray Crystallography*; Kynoch Press: Birmingham, England, 1974; Vol. IV, Table 2.2C.

Table II. Positional Parameters for $PPN[Os_3Br(CO)_{11}]$

atom	x	y	z
Os1	0.10443 (4)	0.12326 (3)	0.00444 (3)
Os2	0.07617 (4)	0.27095 (3)	0.05113 (3)
Os3	0.11388 (4)	0.24602 (3)	0.10325 (3)
Br	0.2908 (1)	0.1118 (1)	−0.0002 (1)
C11	−0.029 (1)	0.1187 (9)	0.0074 (8)
O11	−0.1091 (8)	0.1136 (7)	0.0042 (8)
C12	0.112 (1)	0.0666 (9)	−0.0837 (9)
O12	0.1176 (9)	0.0298 (7)	−0.1352 (7)
C13	0.115 (1)	0.0482 (8)	0.075 (1)
O13	0.1205 (9)	0.0029 (7)	0.1199 (7)
C21	0.205 (1)	0.2568 (8)	−0.0836 (7)
C21	0.2793 (7)	0.2553 (7)	−0.1075 (5)
C22	−0.053 (1)	0.2773 (8)	−0.0153 (7)
O22	−0.1292 (7)	0.2836 (6)	0.0037 (6)
C23	0.031 (1)	0.243 (1)	−0.1455 (8)
O23	0.0022 (8)	0.2242 (8)	−0.2019 (6)
C24	0.082 (1)	0.3752 (8)	−0.056 (1)
O24	0.089 (1)	0.4393 (7)	−0.0605 (8)
C31	0.241 (1)	0.273 (1)	0.0678 (8)
O31	0.3126 (7)	0.2921 (7)	0.0538 (6)
C32	−0.013 (1)	0.216 (1)	0.1272 (7)
O32	−0.0872 (7)	0.2004 (7)	0.1485 (6)
C33	0.099 (1)	0.340 (1)	0.1496 (8)
O33	0.0909 (8)	0.3941 (7)	0.1817 (7)
C34	0.161 (1)	0.1849 (9)	0.1811 (9)
O34	0.1909 (9)	0.1510 (8)	0.2284 (7)
P1	0.5890 (3)	0.1703 (2)	0.4484 (2)
P2	0.5885 (3)	0.1787 (2)	0.6137 (2)
N	0.5830 (8)	0.1476 (6)	0.5315 (6)
C1A	0.5921 (9)	0.2686 (8)	0.4296 (7)
C2A	0.5155 (9)	0.3052 (7)	0.3977 (7)
C3A	0.519 (1)	0.3805 (9)	0.3825 (8)
C4A	0.599 (1)	0.4214 (8)	0.4041 (8)
C5A	0.671 (1)	0.3843 (8)	0.4397 (8)
C6A	0.6704 (9)	0.3097 (8)	0.4505 (8)
C1B	0.4902 (9)	0.1300 (8)	0.3991 (7)
C2B	0.489 (1)	0.1281 (8)	0.3224 (7)
C3B	0.413 (1)	0.0963 (8)	0.2856 (9)
C4B	0.340 (1)	0.0648 (8)	0.3257 (8)
C5B	0.3417 (9)	0.0654 (9)	0.3996 (8)
C6B	0.4189 (9)	0.0966 (8)	0.4387 (8)
C1C	0.6941 (9)	0.1336 (7)	0.4063 (7)
C2C	0.725 (1)	0.0634 (8)	0.4331 (8)
C3C	0.808 (1)	0.0324 (9)	0.4021 (9)
C4C	0.853 (1)	0.069 (1)	0.3465 (9)
C5C	0.821 (1)	0.135 (1)	0.3207 (9)
C6C	0.741 (1)	0.1686 (9)	0.3499 (8)
C1D	0.5960 (9)	0.2780 (7)	0.6206 (7)
C2D	0.524 (1)	0.3211 (8)	0.5913 (8)
C3D	0.529 (1)	0.3977 (8)	0.5873 (8)
C4D	0.614 (1)	0.4319 (9)	0.6129 (9)
C5D	0.687 (1)	0.3902 (8)	0.6423 (9)
C6D	0.678 (1)	0.3138 (9)	0.6464 (8)
C1E	0.692 (1)	0.1432 (8)	0.6597 (7)
C2E	0.767 (1)	0.1210 (8)	0.6164 (8)
C3E	0.850 (1)	0.0945 (9)	0.6503 (8)
C4E	0.858 (1)	0.0934 (9)	0.7253 (9)
C5E	0.783 (1)	0.1159 (9)	0.7665 (8)
C6E	0.697 (1)	0.1393 (8)	0.7363 (7)
C1F	0.486 (1)	0.1500 (8)	0.6651 (7)
C2F	0.4323 (9)	0.1971 (8)	0.7042 (7)
C3F	0.353 (1)	0.171 (1)	0.7417 (8)
C4F	0.328 (1)	0.097 (1)	0.7377 (8)
C5F	0.385 (1)	0.0494 (9)	0.6993 (9)
C6F	0.464 (1)	0.0737 (8)	0.6620 (8)

Table III. Bond Distances (Å) for $PPN[Os_3Br(CO)_{11}]$

	A. Os_3Br Core		
Os1–Os2	2.869 (1)	Os2–Os3	2.886 (1)
Os1–Os3	2.848 (1)	Os1–Br	2.655 (2)
	B. Metal Carbonyls		
Os1–C11	1.89 (2)	C11–O11	1.15 (2)
Os1–C12	1.90 (2)	C12–O12	1.15 (2)
Os1–C13	1.86 (2)	C13–O13	1.16 (2)
Os2–C21	1.94 (2)	C21–O21	1.14 (2)
Os2–C22	1.95 (2)	C22–O22	1.14 (2)
Os2–C23	1.90 (2)	C23–O23	1.15 (2)
Os2–C24	1.88 (2)	C24–O24	1.16 (2)
Os3–C31	1.98 (2)	C31–O31	1.11 (2)
Os3–C32	1.93 (2)	C32–O32	1.16 (2)
Os3–C33	1.91 (2)	C33–O33	1.14 (2)
Os3–C34	1.91 (2)	C34–O34	1.13 (2)
	C. Cation		
P1–N	1.57 (1)	P2–N	1.59 (1)

Table IV. Bond Angles (deg) for $PPN[Os_3Br(CO)_{11}]$

	A. Os_3Br Core		
Os2–Os1–Os3	60.64 (2)	Os3–Os2–C21	96.1 (4)
Os2–Os1–Br	101.40 (5)	Os3–Os2–C22	81.6 (4)
Os2–Os1–C11	85.0 (5)	Os3–Os2–C23	153.7 (5)
Os2–Os1–C12	102.1 (5)	Os3–Os2–C24	101.3 (6)
Os2–Os1–C13	157.3 (6)	Os1–Os3–Os2	60.04 (2)
Os3–Os1–Br	92.14 (5)	Os1–Os3–C31	91.6 (5)
Os3–Os1–C11	93.4 (5)	Os1–Os3–C32	83.4 (5)
Os3–Os1–C12	160.6 (5)	Os1–Os3–C33	164.5 (4)
Os3–Os1–C13	97.4 (5)	Os1–Os3–C34	92.0 (5)
Os1–Os2–Os3	59.32 (2)	Os2–Os3–C31	78.9 (4)
Os1–Os2–C21	81.7 (4)	Os2–Os3–C32	95.5 (4)
Os1–Os2–C22	93.8 (5)	Os2–Os3–C33	105.7 (4)
Os1–Os2–C23	96.7 (5)	Os2–Os3–C34	150.6 (5)
Os1–Os2–C24	159.3 (6)		
	B. Ligand–Metal–Ligand		
Br– s1–C11	173.1 (5)	C22–Os2–C23	90.3 (6)
Br–Os1–C12	82.4 (5)	C22–Os2–C24	90.1 (7)
Br–Os1–C13	83.8 (6)	C23–Os2–C24	103.6 (8)
C11–Os1–C12	93.7 (7)	C31–Os3–C32	173.9 (6)
C11–Os1–C13	91.3 (7)	C31–Os3–C33	91.3 (7)
C12–Os1–C13	100.5 (7)	C31–Os3–C34	94.1 (7)
C21–Os2–C22	175.5 (6)	C32–Os3–C33	92.7 (7)
C21–Os2–C23	90.2 (6)	C32–Os3–C34	89.6 (7)
C21–Os2–C24	94.1 (7)	C33–Os3–C34	103.0 (7)
	C. Metal Carbonyls and Cation		
Os1–C11–O11	175 (2)	Os2–C24–O2j	178 (2)
Os1–C12–O12	177 (2)	Os3–C3–O31	174 (1)
Os1–C13–O1o	178 (2)	Os3–C32–O32	173 (1)
Os2–C21–O21	172 (1)	Os3–C33–O33	175 (1)
Os2–C22–O22	177 (1)	Os3–C3–O34	177 (2)
Os2–C2o–O2o	178 (2)	P1–N–P2	143.9 (8)

After least-squares refinement of all atoms in the structure, several large peaks in the difference Fourier map remained, which indicated the presence of a disordered orientation of the anion. Refinement of the occupancies of the heavy atoms revealed an 11% population of the disordered orientation. Figure 2 illustrates the structure of this orientation as well as its position relative to the major orientation. Attempts to grow crystals of either orientation by using other cations were unsuccessful. Because of the small amount of the disordered orientation, no attempt was made to locate the C and O atoms of the carbonyl ligands.

The large number of variables required that the anion and cation be refined in separate least-squares cycles. After convergence, the hydrogen atoms were added to the list (but not refined) in their idealized positions with a fixed isotropic thermal parameter 20% higher than that of the carbons to which they were bonded. The highest peak in the final difference Fourier map was 3.4 e/Å^3, which was in the region of one of the Os atoms. The positional parameters, bond distances, and bond angles are listed in Tables V–VII, and Figure 3 illustrates the structure of the anion.

Results and Discussion

Syntheses of Monosubstituted Monoanionic Osmium Trimers. The direct reaction of $Os_3(CO)_{12}$ with the PPN salts of the halide ions does not occur at room temperature and leads to mixtures of products at elevated temperatures. Good yields of the desired monosubstituted clusters were obtained at room temperature by the addition of trimethylamine *N*-oxide to the mixture of the PPN halide and $Os_3(CO)_{12}$. Unlike the halide salts, the more nucleophilic anion azide was found to directly react with $Os_3(CO)_{12}$ at room temperature. High yields of the isocyanate-containing

Table V. Positional Parameters for $PPN[Os_3I(CO)_{11}]$

atom	*x*	*y*	*z*
Os1	0.70829 (5)	0.08223 (3)	0.09154 (3)
Os2	0.83969 (4)	0.12102 (3)	−0.02054 (4)
Os3	0.72234 (5)	0.00597 (4)	−0.05071 (4)
Os1′	0.7466 (4)	0.0790 (3)	0.1042 (4)
Os2′	0.7069 (7)	0.0209 (5)	−0.0563 (6)
Os3′	0.8218 (3)	0.1446 (2)	−0.0530 (3)
I	0.77109 (6)	0.16330 (4)	0.22109 (5)
I11	0.9303 (9)	0.0952 (6)	0.0796 (7)
C11	0.601 (1)	0.0501 (8)	0.1272 (9)
O11	0.5352 (8)	0.0300 (6)	0.1496 (7)
C12	0.640 (1)	0.1579 (7)	0.0437 (8)
O12	0.5910 (8)	0.2028 (6)	0.0212 (8)
C13	0.770 (1)	0.0049 (7)	0.1448 (7)
O13	0.8016 (9)	−0.0422 (6)	0.1765 (7)
C21	0.907 (2)	0.071 (1)	0.062 (1)
O21	0.9643 (9)	0.0515 (6)	0.1152 (8)
C22	0.893 (1)	0.2049 (8)	0.019 (1)
O22	0.929 (1)	0.2545 (6)	0.037 (1)
C2o	0.912 (1)	0.0986 (6)	−0.109 (1)
O23	0.953 (1)	0.0856 (7)	−0.1597 (7)
C24	0.752 (1)	0.1705 (8)	−0.092 (1)
O24	0.704 (1)	0.1998 (7)	−0.1381 (8)
C31	0.642 (1)	−0.0629 (8)	−0.021 (1)
O31	0.598 (1)	−0.1061 (6)	0.0020 (7)
C32	0.622 (1)	0.0634 (8)	−0.087 (1)
O32	0.5606 (8)	0.0973 (6)	−0.1121 (7)
C33	0.746 (1)	−0.0195 (7)	−0.158 (1)
O33	0.762 (1)	−0.0341 (6)	−0.2204 (6)
C34	0.828 (1)	−0.0418 (9)	−0.008 (1)
O34	0.8901 (8)	−0.0766 (6)	0.0146 (8)
P1	0.7400 (2)	−0.1733 (2)	0.5708 (2)
N	0.7717 (8)	−0.0980 (5)	0.5532 (6)
P2	0.7567 (2)	−0.0449 (2)	0.4812 (2)
C1A	0.826 (1)	−0.2100 (6)	0.6401 (7)
C2A	0.897 (1)	−0.1685 (6)	0.6732 (8)
C3A	0.965 (1)	−0.1970 (8)	0.728 (1)
C4A	0.961 (4)	−0.2658 (7)	0.747 (1)
C5A	0.892 (1)	−0.3063 (7)	0.715 (1)
C6A	0.826 (1)	−0.2786 (6)	0.6621 (8)
C1B	0.6343 (8)	−0.1742 (6)	0.6180 (8)
C2B	0.601 (1)	−0.1137 (7)	0.6468 (8)
C3B	0.521 (1)	−0.1127 (8)	0.6832 (9)
C4B	0.473 (1)	−0.170 (1)	0.693 (1)
C5B	0.505 (1)	−0.2315 (7)	0.662 (1)
C6B	0.585 (1)	−0.2337 (7)	0.6259 (9)
C1C	0.725 (1)	−0.2277 (7)	0.4816 (9)
C2C	0.643 (1)	−0.2338 (7)	0.440 (1)
C3C	0.636 (2)	−0.273 (1)	0.369 (1)
C4C	0.708 (3)	−0.304 (1)	0.340 (1)
C5C	0.793 (2)	−0.295 (1)	0.380 (1)
C6C	0.801 (1)	−0.2584 (8)	0.4546 (9)
C1D	0.662 (1)	−0.0627 (6)	0.4096 (7)
C2D	0.574 (1)	−0.0575 (8)	0.4352 (8)
C3D	0.499 (1)	−0.0747 (7)	0.3841 (9)
C4D	0.507 (1)	−0.0970 (7)	0.308 (1)
C5D	0.595 (1)	−0.1038 (8)	0.2812 (8)
C6D	0.671 (1)	−0.0859 (8)	0.3313 (8)
C1E	0.736 (1)	0.0386 (6)	0.5233 (8)
C2E	0.758 (1)	0.0505 (7)	0.6049 (9)
C3E	0.745 (1)	0.1135 (8)	0.635 (1)
C4E	0.715 (1)	0.1664 (7)	0.588 (1)
C5E	0.692 (1)	0.1561 (8)	0.507 (1)
C6E	0.702 (1)	0.00923 (8)	0.473 (1)
C1F	0.858 (1)	−0.0380 (6)	0.4285 (7)
C2F	0.930 (1)	−0.0818 (7)	0.4484 (8)
C3F	1.006 (1)	−0.0783 (7)	0.4060 (9)
C4F	1.011 (1)	−0.0316 (9)	0.3447 (9)
C5F	0.939 (1)	0.012 (1)	0.3260 (9)
C6F	0.864 (1)	0.0080 (8)	0.3665 (9)

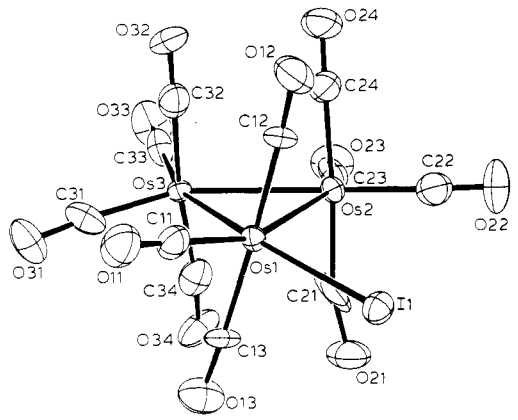

Figure 3. Structure of the anion in $PPN[Os_3I(CO)_{11}]$, using 50% probability ellipsoids.

Table VI. Bond Distances (Å) for $PPN[Os_3I(CO)_{11}]$

	A. Os_3I Core		
Os1–Os2	2.901 (2)	Os2–Os3	2.854 (2)
Os1–Os3	2.818 (2)	Os1–I	2.764 (2)
	B. Metal Carbonyls		
Os1–C11	1.85 (2)	C11–O11	1.13 (2)
Os1–C12	1.92 (1)	C12–O12	1.17 (2)
Os1–C13	1.94 (1)	C13–O13	1.14 (2)
Os2–C21	1.89 (2)	C21–O21	1.22 (3)
Os2–C22	1.91 (2)	C22–O22	1.13 (2)
Os2–C23	1.94 (1)	C23–O23	1.11 (2)
Os2–C24	1.93 (2)	C24–O24	1.14 (2)
Os3–C31	1.88 (2)	C31–O31	1.16 (2)
Os3–C3	1.91 (2)	C32–O32	1.17 (2)
Os3–C33	1.92 (2)	C33–O33	1.11 (2)
Os3–C34	1.88 (2)	C34–O34	1.18 (2)
	C. Cation		
P1–N	1.58 (1)	P2–N	1.59 (1)

cluster $[Os_3(NCO)(CO)_{11}]^-$ were obtained, presumably through nucleophilic attact at a carbonyl carbon followed by a reaction analogous to the Curtius rearrangement of acyl azides.[12] All compounds gave acceptable elemental analytical data.

The infrared spectra of all four anionic clusters exhibited a complex pattern in the terminal carbonyl region. The spectra of the three clusters where X = Cl, Br, and NCO were nearly identical, whereas the energy of several absorptions of the iodo cluster differed slightly (see Experimental Section). The complex patterns yielded little additional information about the solution structures except that all the CO ligands were terminally coordinated to the metals. The ^{13}C NMR spectroscopy, which did yield conclusive information about the structures in solution, will be described following discussion of the solid-state structures of the bromide- and iodide-containing clusters.

Structure of $[Os_3Br(CO)_{11}]^-$. The structure consists of ordered, separated cations and anions. The Os–Os bond distances (average = 2.868 (19) Å) are slightly smaller than those found in $Os_3(CO)_{12}$ itself.[13] The bromide ligand is bound to Os1 in the axial position, as illustrated in Figure 1. The Os1–Br bond distance of 2.655 (2) Å is not unusual. The 11 carbonyls are coordinated to the osmium atoms as linear, terminal ligands. There is no indication of close contacts between the carbons and adjacent osmium atoms that might indicate the formation of semibridging interactions.

A noteworthy feature of the structure of the anion is the concerted twist of the three ML_4 fragments. If we momentarily ignore the difference between the Br and CO ligands, this has the effect of lowering the symmetry of the M_3L_{12} cluster from D_{3h} (as it is in $Os_3(CO)_{12}$) to D_3. While the individual values of the Os–Os–L angles give some indication of the degree of twisting, the most accurate representation comes from the calculation of the angle of intersection between the Os_3 plane and the individual Os–C(eq)–C(eq) planes. For Os(1–3), these values are 10.2, 12.5, and 10.5°, respectively.

Table VII. Bond Angles (deg) for $PPN[Os_3I(CO)_{11}]$

	A. Os_3I Core		
Os2–Os1–Os3	59.85 (4)	Os3–Os2–C21	89.4 (7)
Os2–Os1–I	98.86 (5)	Os3–Os2–C22	163.8 (5)
Os2–Os1–C11	158.9 (4)	Os3–Os2–C23	93.1 (4)
Os2–Os1–C12	83.5 (5)	Os3–Os2–C24	85.9 (5)
Os2–Os1–C13	100.7 (4)	Os1–Os3–Os2	61.52 (3)
Os3–Os1–I	155.80 (4)	Os1–Os3–C31	93.7 (5)
Os3–Os1–C11	102.6 (4)	Os1–Os3–C32	80.7 (5)
Os3–Os1–C12	97.9 (4)	Os1–Os3–C33	162.2 (4)
Os3–Os1–C13	84.3 (4)	Os1–Os3–C34	93.9 (5)
Os1–Os2–Os3	58.62 (4)	Os2–Os3–C31	154.2 (5)
Os1–Os2–C21	74.6 (7)	Os2–Os3–C32	91.5 (5)
Os1–Os2–C22	106.0 (5)	Os2–Os3–C33	102.1 (4)
Os1–Os2–C23	150.3 (4)	Os2–Os3–C34	82.1 (5)
Os1–Os2–C24	94.5 (5)		
	B. Ligand–Metal–Ligand		
I–Os1–C11	100.4 (4)	C22–Os2–C23	102.9 (7)
I–Os1–C12	90.2 (4)	C22–Os2–C24	90.6 (7)
I–Os1–C13	89.1 (4)	C23–Os2–C24	91.9 (6)
C11–Os1–C12	87.9 (7)	C31–Os3–C32	91.3 (7)
C11Os1–C13	88.1 (6)	C31–Os3–C33	103.2 (7)
C12–Os1–C13	175.8 (6)	C31–Os3–C34	93.3 (7)
C21–Os2–C22	91.1 (8)	C32–Os3–C33	93.4 (7)
C21–Os2–C23	98.3 (9)	C32–Os3–C34	173.2 (7)
C21–Os2–C24	169.0 (9)	C33–Os3–C34	90.4 (7)
	C. Metal Carbonyls and Cation		
Os1–C11–O11	179 (1)	Os2–C24–O24	176 (1)
Os1–C12–O12	172 (1)	Os3–C31–O31	175 (2)
Os1–C13–O13	176 (1)	Os3–C32–O32	177 (1)
Os2–C21–O21	165 (2)	Os3–C33–O33	179 (2)
Os2–C22–O22	173 (2)	Os3–C34–O34	174 (1)
Os2–C23–O23	179 (2)	P1–N–P2	136.7 (7)

Structure of $[Os_3I(CO)_{11}]^-$. The structure consists of well-separated anions and cations, the former exhibiting some disorder. Figure 2 illustrates the position of the second orientation of the triosmium ring and, surprisingly, shows that the iodide is bridging from Os11 to Os33. The elongated Os11–Os33 distance of 3.19 (1) Å would be consistent with adding two additional electrons to the cluster framework; however, the inability to locate the carbonyl ligands in this minor orientation precludes any meaningful discussion of this point. The two metal–metal bond distances are Os11–Os22 = 2.91 (1) Å and Os22–Os33 = 2.95 (1) Å. The osmium–iodide bond distances are Os11–I11 = 2.78 (1) Å and Os33–I11 = 2.77 (1) Å. From this point on the discussion will be concerned only with the major orientation shown in Figure 3.

The Os–Os bond distances average to 2.858 (42) Å, which is essentially the same as that found in the bromide structure. The significant difference between the two structures is the location of the halide ligand. Unlike the bromide, the iodide is located in an equatorial position with an Os1–I bond distance of 2.764 (1) Å. As in $[Os_3Br(CO)_{11}]^-$, the carbonyls are coordinated to the osmium atoms as linear, terminal ligands. There is no indication of close contacts between the carbons and adjacent osmium atoms that might indicate the formation of semibridging interactions. Despite the change of the halide position, the ML_4 groups are also tilted in the iodide structure. The angles between the three Os–C(eq)–C(eq) (or I) planes and the Os_3 plane are 16.1, 10.3, and 9.4°, respectively.

Comparison of Structures. A large number of $M_3(CO)_{12}$ clusters substituted with one or more neutral ligands have been structurally characterized.[14–35] An excellent summary of the

(12) Fjare, D. E.; Jensen, J. A.; Gladfelter, W. L. *Inorg. Chem.* **1983**, *22*, 1774.
(13) Churchill, M. R.; DeBoer, B. G. *Inorg. Chem.* **1977**, *16*, 878.
(14) Bruce, M. I.; Matisons, J. G.; Skelton, B. W.; White, A. H. *J. Chem. Soc., Dalton Trans.* **1983**, 2375.
(15) Bruce, M. I.; Matisons, J. G.; Patrick, J. M.; White, A. H.; Willis, A. C. *J. Chem. Soc., Dalton Trans.* **1985**, 1223.
(16) Forbes, E. J.; Goodhand, N.; Jones, D. L.; Hamor, T. A. *J. Organomet. Chem.* **1979**, *182*, 143.
(17) Coleman, A. W.; Jones, D. F., Dixneuf, P. H.; Brisson, C.; Bonnet, J.-J.; Lavigne, G. *Inorg. Chem.* **1984**, *23*, 952.

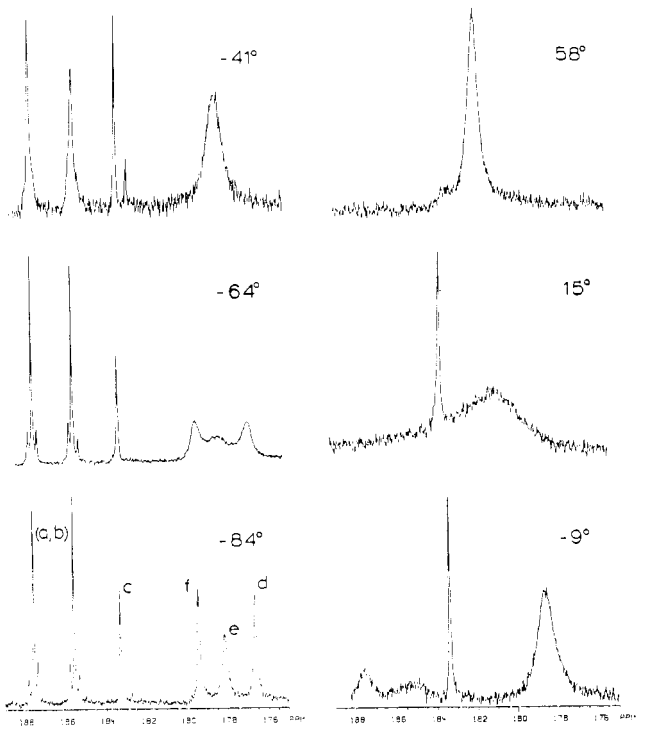

Figure 4. Variable-temperature ^{13}C NMR spectra of PPN[Os_3(NC-O)$(CO)_{11}$].

structures of $M_3(CO)_{12-n}L_n$ (n = 1–3) is included in the recent studies of Bruce and co-workers.[33-35] The dividing line determining whether substitution occurs at an axial vs an equatorial position is well-defined. Unidentate phosphine, arsine, and related ligands that have branching on the ligating atom always substitute for a CO in the equatorial position. The preference of these more sterically demanding ligands for this site is a result of reduced repulsions between the ligand and the carbonyls on the adjacent metals. In the equatorial position the critical interaction is the result of one 1,2-diequatorial overlap, whereas two 1,2-diaxial contacts exist when the ligand is in the axial position. Ligands without branching at the ligating atom (CH_3CN and t-$(CH_3)_3CNC$) exhibit a preference for bonding in the axial position.[28-30] The electronic preference for substitution at this site is probably small and likely due to the placement of a less effective π-accepting ligand trans to the remaining axial CO.

The series of anionic clusters reported in this paper follows the trend just described. With the three smaller anions, NCO^-, Cl^- and Br^-, axial substitution is observed, whereas the largest anion, iodide, substitutes in the equatorial position. Regardless of the substitution site, these two anionic clusters along with all the neutral, monosubstituted clusters exhibit a twisting of each of the ML_4 groups, lowering the overall symmetry of the cluster to D_3. In terms of the magnitude of interligand repulsions, several different studies have shown[36-39] that the D_3 structure lies between the least crowded, D_{3h}, M_3L_{12} structure and the close-packed, C_{2v} form.

Two structurally characterized clusters of ruthenium having 10 CO ligands and 1 anionic ligand have been reported. In $[Ru_3(O_2CH)(CO)_{10}]^-$[40] and $\{[Ru_3(CN)(CO)_{10}]_2\}^{2-}$[41] the anions

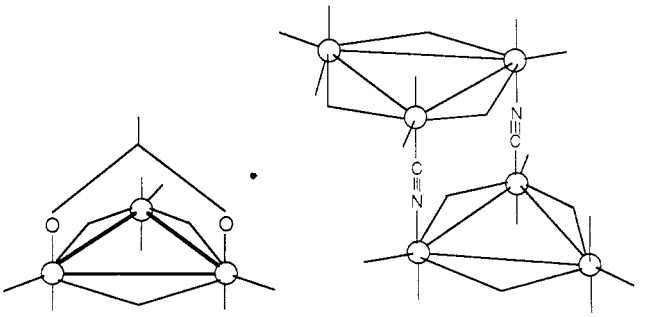

$[Ru_3(O_2CCH)(CO)_{10}]^-$ $\{[Ru_3(CN)(CO)_{10}]_2\}^{2-}$

reside in axial positions; however, the bridging nature of the anionic ligand may force the observed geometry. It is interesting that both of these structures contain three bridging CO's in the equatorial plane.

Finally, it is noteworthy that, among the CO ligands in both $[Os_3Br(CO)_{11}]^-$ and $[Os_3I(CO)_{11}]^-$, no systematic lengthening of the M–C bonds can be observed. This observation suggests that the CO labilization effect caused by halides does not involve a destabilization of the ground-state structure.

^{13}C NMR Spectroscopic Studies. A monosubstituted cluster can have a ligand occupy either an axial or equatorial position. For $Os_3(L)(CO)_{11}$, the two possible structures are shown as follows:

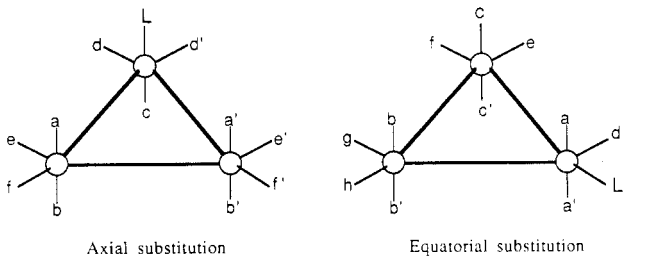

Axial substitution Equatorial substitution

If the ligand were axial, one would expect to see six signals in the carbonyl region of the spectrum at the low-temperature limit. This has been observed[42] in the related neutral cluster $Os_3(CO)_{11}$-(CN-n-Bu), which exhibits five carbonyl signals with intensity ratios 2:2:1:4:2 at low temperature (two pairs of carbonyls are accidentally degenerate). In contrast to this behavior, the low-temperature spectrum of $Os_3(CO)_{11}PEt_3$, which is equatorially

(18) Lavigne, G.; Lugan, N.; Bonnet, J.-J. *Acta Crystallogr.* **1982**, *B38*, 1911.
(19) Bruce, M. I.; Hambley, T. W.; Nicholson, B. K.; Snow, M. R. *J. Organomet. Chem.* **1982**, *235*, 83.
(20) Gallucci, J.; Gilbert, K. B.; Hsu, W.-L.; Shore, S. G. *Cryst. Struct. Commun.* **1982**, *11*, 385.
(21) Roberts, P. J.; Trotter, J. *J. Chem. Soc.* **1970**, 3246.
(22) Roberts, P. J.; Trotter, J. *J. Chem. Soc.* **1971**, 1479.
(23) Benfield, R. E.; Johnson, B. F. G.; Raithby, P. R.; Sheldrick, G. M. *Acta Crystallogr.* **1978**, *B34*, 666.
(24) Bruce, M. I.; Hambley, T. W.; Nicholson, B. K.; Snow, M. R. *J. Organomet. Chem.* **1982**, *235*, 83.
(25) Ehrenreich, W.; Herberhold, M.; Süss-Fink, G.; Klein, H.-P.; Thewalt, U. *J. Organomet. Chem.* **1983**, *248*, 171.
(26) Gieren, A.; Hübner, T.; Herberhold, M.; Guldner, K.; Süss-Fink, G. *Z. Anorg. Allg. Chem.* **1986**, *538*, 21.
(27) Cartwright, S.; Clucas, J. A.; Dawson, R. H.; Foster, D. F.; Harding, M. M.; Smith, A. K. *J. Organomet. Chem.* **1986**, *302*, 403.
(28) Bruce, M. I.; Matisons, J. G.; Wallis, R. C.; Patrick, J. M.; Skelton, B. W.; White, A. H. *J. Chem. Soc., Dalton Trans.* **1983**, 2365.
(29) Bruce, M. I.; Pain, G. N.; Hughes, C. A.; Patrick, J. M.; Skelton, B. W.; White, A. H. *J. Organomet. Chem.* **1986**, *307*, 343.
(30) Dawson, P. A.; Johnson, B. F. G.; Lewis, J.; Puga; Raithby, P. R.; Rosales, M. J. *J. Chem. Soc., Dalton Trans.* **1982**, 233.
(31) DeBoer, J. J.; Van Doorn, J. A.; Masters, C. *J. Chem. Soc., Chem. Commun.* **1978**, 1005.
(32) Chin-Choy, T.; Keder, N. L.; Stucky, G. D.; Ford, P. C. *J. Organomet. Chem.* **1988**, *346*, 225.
(33) Bruce, M. I.; Liddell, M. J.; Hughes, C. A.; Skelton, B. W.; White, A. H. *J. Organomet. Chem.* **1988**, *347*, 157.
(34) Bruce, M. I.; Liddell, M. J.; Hughes, C. A.; Patrick, J. M.; Skelton, B. W.; White, A. H. *J. Organomet. Chem.* **1988**, *347*, 157.
(35) Bruce, M. I.; Liddell, M. J.; Shawkataly, O. B.; Hughes, C. A.; Skelton, B. W.; White, A. H. *J. Organomet. Chem.* **1988**, *347*, 157.
(36) Johnson, B. F. G. *J. Chem. Soc., Chem. Commun.* **1976**, 211.
(37) Johnson, B. F. G.; Benfield, R. E. *J. Chem. Soc., Dalton Trans.* **1978**, 1554.
(38) Johnson, B. F. G.; Benfield, R. E. *J. Chem. Soc., Dalton Trans.* **1980**, 1743.
(39) Lauher, J. W. *J. Am. Chem. Soc.* **1986**, *108*, 1521.
(40) Darensbourg, D. J.; Pala, M.; Waller, J. *Organometallics* **1983**, *2*, 1285.
(41) Lavigne, G.; Lugan, N.; Bonnet, J.-J. *J. Chem. Soc., Chem. Commun.* **1987**, 957.
(42) Mays, M. J.; Gravens, P. D. *J. Chem. Soc., Dalton Trans.* **1980**, 911.

Scheme I. Exchange of Equatorial Ligands

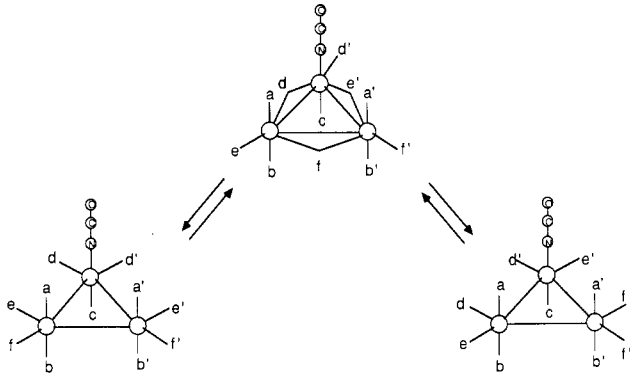

Scheme II. Pairwise Bridge–Terminal CO Exchange

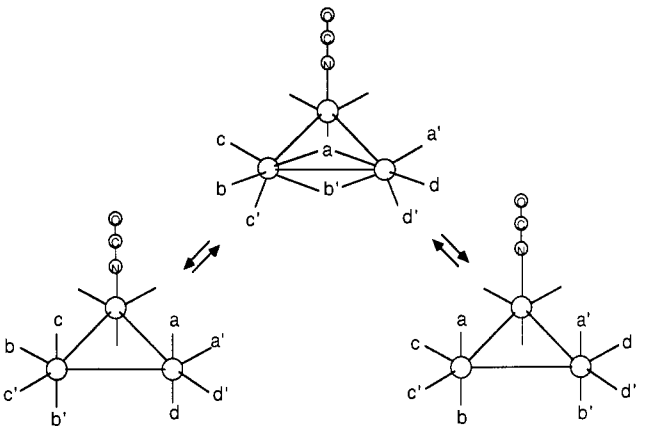

substituted,[43] exhibits the eight expected resonances. The site of substitution has been shown to determine the CO-scrambling mechanism.

The variable-temperature ^{13}C NMR spectra for $PPN[Os_3(NCO)(CO)_{11}]$ are shown in Figure 4. The low temperature (−84 °C) limiting spectrum exhibits six resonances with relative intensities 2:2:1:2:2:2, consistent with axial substitution. The signal of intensity 1 at 183.3 ppm is assigned to the unique carbonyl c, which is axial and trans to the isocyanate ligand. The lowfield signals at 187.5 and 185.6 ppm are assigned to the pairs of axial carbonyls a and b, on the basis of ^{13}C–^{13}C coupling of ca. 35 Hz, which is frequently observed for trans-$Os(CO)_2$ groups. The signals at 179.4, 178.1, and 176.6 ppm are assigned to the three pairs of equatorial carbonyls d, e, and f. A unique assignment of the resonance at 178.1 ppm to carbonyl e is based on observations of the fluxional process described below. In analogy to the equatorial CO region, where the CO bound to the same metal as the NCO group is furthest upfield, we suggest that the resonance at 176.6 ppm is due to carbonyl d. Finally, the isocyanate carbon appears at 124.97 ppm.

Upon warming of the sample to −64 °C, the three equatorial carbonyl signals broaden. Coalescence to a single broad peak of relative intensity 6 at 178.4 ppm occurs at −40 °C. The downfield signals remain relatively unchanged, as does the isocyanate carbon resonance. These data are consistent with an in-plane scrambling of the six equatorial carbonyls via the so-called merry-go-round process,[44] shown in Scheme I. A close inspection of the −64 °C spectrum of $PPN[Os_3(NCO)(CO)_{11}]$ indicates that the signal at 178.1 ppm broadens before the other two equatorial signals. The merry-go-round process would always exchange one carbonyl of d and f with an equivalent one, while carbonyls e would always exchange with nonequivalent carbonyls. This mechanism requires faster collapse of e, and thus the signal at 178.1 ppm is assigned to e, and the remaining signal at 179.4 ppm, to f.

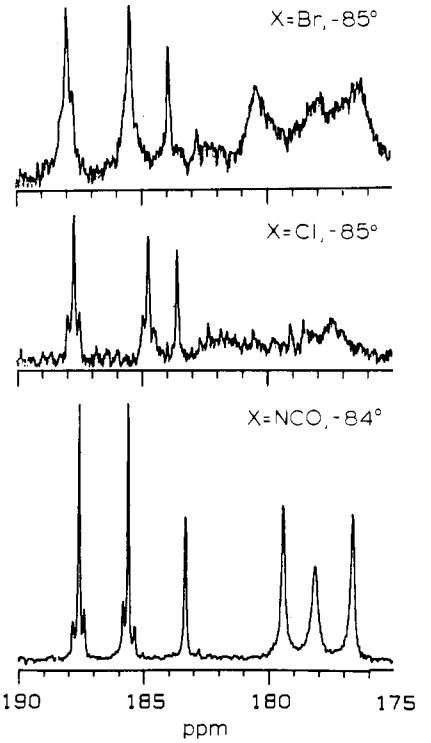

Figure 5. ^{13}C NMR spectra of the carbonyl region of $PPN[Os_3X(CO)_{11}]$ in $CDCl_3$.

Scheme III. Trigonal-Twist Mechanism Incorporating Axial CO Groups

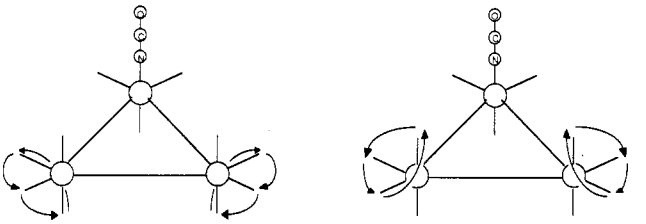

Scheme IV. Trigonal-Twist Mechanism Involving $Os(NCO)(CO)_3$

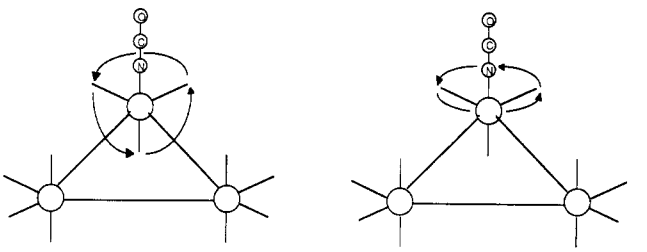

Further warming of $[Os_3(NCO)(CO)_{11}]^-$ to −9 °C results in the onset of a second exchange process, as indicated by broadening of the two axial signals due to a and b. The unique carbonyl resonance remains unchanged. Pairwise bridge–terminal CO exchange[45] around the $Os_2(CO)_8$ unit could account for the involvement of a and b in the exchange process (Scheme II). Alternatively, a trigonal-twist mechanism[46-49] on the two $Os(CO)_4$ groups would also account for the observed broadening (Scheme III). The spectra shown at −41 and −9 °C show broadening of the peak at 185.6 ppm occurs slightly faster than that the reso-

(43) Johnson, B. F. G.; Lewis, J.; Reichert, B. E.; Schorpp, K. T. *J. Chem. Soc., Dalton Trans.* **1976**, 1403.
(44) Band, E.; Muetterties, E. L. *Chem. Rev.* **1978**, *78*, 639.
(45) Adams, R. D.; Cotton, F. A. *J. Am. Chem. Soc.* **1973**, *95*, 6589.
(46) Bryan, E. G.; Forster, A.; Johnson, B. F. G.; Lewis, J.; Matheson, T. W. *J. Chem. Soc., Dalton Trans.* **1978**, 196.
(47) Gavens, P. D.; Mays, M. J. *J. Organomet. Chem.* **1978**, *162*, 389.
(48) Bruce, M. I.; Schultz, D.; Wallis, A. C.; Redhouse, A. D. *J. Organomet. Chem.* **1979**, *169*, C15.
(49) Johnson, B. F. G.; Lewis, J.; Mace, J.; Raithby, P. R.; Stevens, R. E.; Gladfelter, W. L. *Inorg. Chem.* **1984**, *23*, 1600.

nance at 187.5 ppm. Either mechanism could account for these observations.

Warming the sample to 15 °C coalesces all of the signals, with the exception of c, to a broad singlet at 180.5 ppm. At 58 °C, the unique carbonyl resonance finally coalesces with the others, indicating its involvement in the exchange via a trigonal-twist process. At this temperature, the signal for the isocyanate carbon also broadens and decreases in intensity. It is possible that the $Os(NCO)(CO)_2$ group also undergoes a twist, placing the NCO ligand in an equatorial position, which is likely to have a different chemical shift (Scheme IV).

Figure 5 shows the low-temperature spectra for $[Os_3X(CO)_{11}]^-$ (X = Cl, Br, NCO). Both the chloride and bromide clusters exhibit the same six-line pattern as observed for the isocyanate cluster, although the upfield (equatorial) signals are broadened by exchange at the lowest temperatures studied. The three downfield signals can be assigned as the axial carbonyls on the basis of chemical shift and the $^{13}C-^{13}C$ coupling of 36 Hz for X = Cl and 33 Hz for X = Br. The relative intensities of these peaks are 2:2:1, consistent with occupation of an axial position by the halide.

The fluxional behavior of the chloride- and bromide-containing clusters was found to be similar to that of the isocyanate cluster. The low-temperature spectrum for $[Os_3Cl(CO)_{11}]^-$ (Figure 5) indicates that considerable in-plane exchange of the equatorial carbonyls is occurring, even at −85 °C. At −60 °C, the equatorial carbonyl signals have coalesced to one peak, consistent with the merry-go-round process. At −35 °C, the axial signals broaden, although the unique signal at 183.7 ppm remains sharp. All peaks have broadened into an average signal by −10 °C, which sharpens at 25 °C.

As with the case for chloride, the equatorial exchange in $[Os_3Br(CO)_{11}]^-$ is already occurring at −85 °C (Figure 5). By −70 °C, the equatorial signals have coalesced, and the axial carbonyl signals, including that for the unique CO, begin to broaden. This indicates that the first process for $[Os_3Br(CO)_{11}]^-$ is the in-plane scrambling of the equatorial carbonyl ligands via the merry-go-round process. For this cluster, however, the unique axial CO appears to exchange with the others. Coalescence of all signals is nearly complete by −25 °C, and by 25 °C the signal has sharpened to an averaged peak at 182.8 ppm. The observation that the carbonyl trans to the Br undergoes exchange at the same time as do the other axial carbonyls implies that the relative barrier for the trigonal twist of the $OsBr(CO)_2$ group is lower than those for the chloride- and isocyanate-containing clusters. This would seem to fit into the trend (continued as well with the iodo cluster) of decreasing activation energies for this twist of the $OsX(CO)_2$ unit with increasing size of the anion.

If the cluster were equatorially substituted, eight resonances of relative intensity 2:2:2:1:1:1:1:1 would be expected in the limiting spectrum. Figure 6 shows the low-temperature (−90 °C) spectrum of $[Os_3(I)(CO)_{11}]^-$, which exhibits seven signals of relative intensity 2:2:2:1:1:2:1. The signals at 193.1, 189.1, and 184.5 ppm can be assigned to the three pairs of axial carbonyls, again on the basis of chemical shift. There is no evidence for a second isomer such as that found in the solid state. Unfortunately, the low signal to noise and the broadening from the exchange process preclude the observation of the $^{13}C-^{13}C$ coupling, which would have offered a more conclusive assignment. The equatorial signal at 173.5 ppm, which also integrates to 2 carbons, must be the result of accidental overlap.

At higher temperatures, it was found that all seven signals of $[Os_3I(CO)_{11}]^-$ began to broaden at the same time until, at −40 °C, all have essentially disappeared into the base line (Figure 6). They reappear as one averaged signal at 8 °C. With the iodo ligand situated in the equatorial position, the merry-go-round exchange process common to the other clusters is blocked. Once the $OsI(CO)_2$ twists the iodo ligand into the axial position, however, the merry-go-round process could readily exchange the equatorial ligands. As mentioned above, the barrier for the trigonal twist of the $OsX(CO)_2$ is lowered as one proceeds from NCO through Br. It is reasonable to anticipate a continuation of this trend to the iodo cluster. An additional process must also be working that results of the averaging of the axial carbonyls on the $Os(CO)_4$ fragments. Here also, the trend in carbonyl exchange on the $Os(CO)_3$ groups of the $Os(CO)_4$ fragments also leads to lower temperatures as X ranges from NCO to Cl to Br. It is not unreasonable to anticipate that this process occurs about the same time as those just described, resulting in the coalescence of all CO ligands at once.

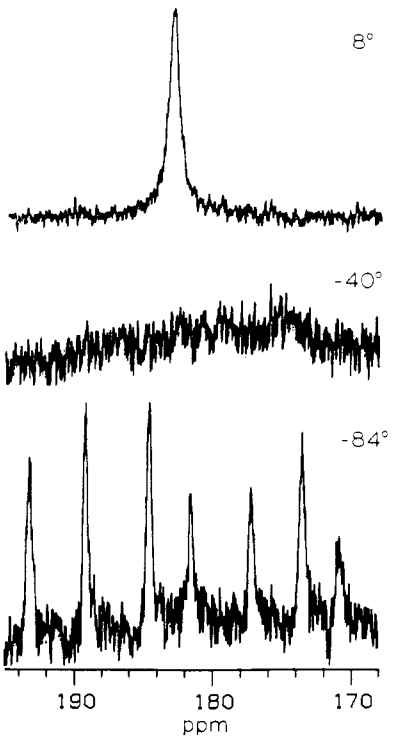

Figure 6. Variable-temperature ^{13}C NMR spectra of $PPN[Os_3I(CO)_{11}]$.

Among the other examples of monosubstituted clusters having neutral ligands, the in-plane merry-go-round exchange mechanism is not observed. Ample precedence for this process does exist among clusters containing ligands that bridge between two axial sites. Observation of such a process was first made on the neutral clusters $Ru_3(1,2\text{-diazene})(CO)_{10}$[50] and $Os_3(1,2\text{-diazene})(CO)_{10}$.[51] The carboxylate-bridged cluster $[Ru_3(O_2CH)(CO)_{10}]^-$[40] and the dimethylformamido-bridged cluster $\{Ru_3[C(O)N(CH_3)_2](CO)_{10}\}^-$,[52] both of which contain three bridging carbonyls in the equatorial plane, exhibit the in-plane scrambling. Especially relevant to this study was that $\{Os_3[C(O)N(CH_3)_2](CO)_{10}\}^-$ follows this same scrambling pattern despite the fact that the structure contains no bridging carbonyls.[53]

Summary

We have prepared and fully characterized the monosubstituted anionic clusters having the formula $[Os_3X(CO)_{11}]^-$ for X = NCO, Cl, Br, and I. Single-crystal X-ray crystallographic analysis of $PPN[Os_3Br(CO)_{11}]$ ambiguously locates the bromide in the axial position, while the iodide in $PPN[Os_3I(CO)_{11}]$ resides in the equatorial plane of the three metals. Both structures undergo a twisting of the OsL_4 fragments as a result of the steric congestion introduced by the added ligand. It is proposed that the site of substitution is a compromise between the electronic forces, which favor substitution of the axial CO, and the steric forces, which favor placing the larger ligand in an equatorial site. The solution structures of each of the clusters were found to be the same as in the solid state, and the fluxional processes were studied. For

(50) Cotton, F. A.; Hanson, B. E.; Jamerson, J. D. *J. Am. Chem. Soc.* **1977**, *99*, 6588.
(51) Cotton, F. A.; Hanson, B. E. *Inorg. Chem.* **1977**, *16*, 2820.
(52) Mayr, A.; Lin, Y. C.; Boag, N. M.; Kampe, C. E.; Knobler, C. B.; Kaesz, H. D. *Inorg. Chem.* **1984**, *23*, 4640.
(53) Mayr, A.; Lin, Y. C.; Boag, N. M.; Kaesz, H. D. *Inorg. Chem.* **1982**, *21*, 1704.

the clusters where X = NCO, Cl, and Br, the lowest temperature exchange process averages all of the equatorial sites. Involvement of the axial carbonyls in this process occurs via a series of trigonal-twist steps and/or pairwise bridge–terminal CO-exchange steps. With $[Os_3I(CO)_{11}]^-$, all of the carbonyls undergo exchange at the same temperature, possibly through a rate-limiting trigonal twist of the $OsI(CO)_2$ group.

Acknowledgment. This research was supported by a grant from the National Science Foundation (NSF-8714326).

Registry No. $PPN[Os_3Cl(CO)_{11}]$, 119909-83-0; $PPN[Os_3Br(CO)_{11}]$, 119909-85-2; $PPN[Os_3I(CO)_{11}]$, 119909-87-4; $Os_3(CO)_{12}$, 15696-40-9; Me_3NO, 1184-78-7; $PPN[Os_3(NCO)(CO)_{11}]$, 119945-41-4; $PPN(N_3)$, 38011-36-8; CO, 630-08-0.

Supplementary Material Available: Listings of positional and thermal parameters for H atoms, temperature factors, complete bond distances and angles, and crystallographic data (26 pages); tables of calculated and observed structure factors (71 pages). Ordering information is given on any current masthead page.

Contribution from the Departamento de Química Inorgánica-Instituto de Ciencia de Materiales, Universidad de Sevilla-CSIC, 41071 Sevilla, Spain

Pyrrolyl, Hydroxo, and Carbonate Organometallic Derivatives of Nickel(II). Crystal and Molecular Structure of $[Ni(CH_2C_6H_4\text{-}o\text{-}Me)(PMe_3)(\mu\text{-}OH)]_2\cdot 2,5\text{-}HNC_4H_2Me_2$

Ernesto Carmona,* José M. Marín, Pilar Palma, Margarita Paneque, and Manuel L. Poveda

Received October 12, 1988

Pyrrolyl–organometallic derivatives of Ni(II), of composition $Ni(R)(NC_4H_2X_2)(PMe_3)_2$ (X = H (**1a–5a**), 2,5-Me (**1b–5b**); R = Me (**1**), CH_2SiMe_3 (**2**), CH_2CMe_3 (**3**), CH_2CMe_2Ph (**4**), 2,4,6-$C_6H_2Me_3$ (**5**)), have been obtained by treatment of the complexes *trans*-$Ni(R)Cl(PMe_3)_2$ with the sodium salt of the pyrrolyl ligand. The action of wet CO_2 upon solutions of **2a,b** provides the carbonate $Ni_2(CH_2SiMe_3)_2(CO_3)(PMe_3)_3$ (**10**), possibly through the intermediacy of a dimeric hydroxide, $[Ni(CH_2SiMe_3)(PMe_3)(\mu\text{-}OH)]_2$ (**6**). Hydroxides related to **6**, $[Ni(R)(PMe_3)(\mu\text{-}OH)]_2$ (R = CH_2CMe_2Ph (**7**), $CH_2C_6H_5$ (**8**)), have been produced by reacting the corresponding monoalkyl chlorides with powdered NaOH and have been shown to react with CO_2 with formation of carbonates analogous to **10**, $Ni_2R_2(CO_3)(PMe_3)_3$ (R = CH_3 (**9**), CH_2SiMe_3 (**10**), $CH_2C_6H_5$ (**11**), C_6H_5 (**12**)). The hydroxides readily form solid-state adducts, when crystallized in the presence of pyrrole or 2,5-dimethylpyrrole. NMR studies show these adducts are completely dissociated in solution, but an O···H–N hydrogen-bonding interaction exists in the solid state, as revealed by the results of an X-ray structural determination, carried out with the *o*-methylbenzyl complex $[Ni(CH_2C_6H_4\text{-}o\text{-}Me)(PMe_3)(\mu\text{-}OH)]_2\cdot 2,5\text{-}HNC_4H_2Me_2$. The crystals are monoclinic, space group $C2/c$, with cell dimensions a = 15.598 (6) Å, b = 12.655 (7) Å, c = 17.705 (6) Å, β = 111.72 (4)°, V = 3243.7 Å^3, and Z = 4. The structure consists of dinuclear $Ni_2(\eta^1\text{-}CH_2C_6H_4\text{-}o\text{-}Me)_2(PMe_3)_2(\mu\text{-}OH)_2$ molecules and of 2,5-dimethylpyrrole molecules of crystallization, all of them showing crystallographic 2-fold symmetry. The Ni dimers have dihedral geometry, with the Ni atoms situated in a distorted square-planar environment.

Introduction

Numerous studies have been reported concerning the carbonylation of nickel–carbon bonds.[1,2] Less well studied, although of increasing interest, is the analogous carboxylation reaction.[3] Recent work by Yamamoto and co-workers has shown that the possibility of reductive elimination at the metal center in complexes $Ni(R)XL_2$ (R = alkyl or aryl group), following carbonylation depends, among other factors, upon the strength of the Ni–X bond.[4] The same arguments apply probably to the insertion of carbon dioxide but this process is less well documented. On the other hand, the reactions of carbon dioxide with transition-metal compounds are very often complicated by the unpredictable effect of small amounts of water that accompany CO_2 and that are difficult to remove completely. This is in fact a pervasive feature of carbon dioxide chemistry and leads frequently to the formation of hydroxo or carbonate complexes.[5]

As part of continuing studies on the organometallic chemistry of nickel, we have carried out the preparation of some alkyl and aryl complexes, $NiR(NC_4H_2X_2)(PMe_3)_2$, containing the pyrrolyl group. The study of their reactions with CO and CO_2 are the subject of this paper. As discussed below, insertion of carbon monoxide is generally observed, but for carbon dioxide, formation of the binuclear carbonates, $Ni_2R_2(PMe_3)_3(\mu\text{-}CO_3)$, takes place. The latter reaction does not have general application, but a general route to carbonates of this type, through the intermediacy of hydroxo-bridged species, $[NiR(PMe_3)(\mu\text{-}OH)]_2$, has been developed.

Results and Discussion

η^1-*N*-Pyrrolyl Complexes, $Ni(R)(NC_4H_2X_2)(PMe_3)_2$ (1–5). Treatment of diethyl ether solutions of alkyl or aryl complexes of Ni(II) of composition *trans*-$Ni(R)Cl(PMe_3)_2$, with the sodium salt of pyrrole or 2,5-dimethylpyrrole, $NaNC_4H_2X_2$ (X = H, Me), provides yellow crystalline derivatives, $Ni(R)(NC_4H_2X_2)(PMe_3)_2$ (**1–5**) as shown in eq 1. Spectroscopic studies clearly indicate

$$Ni(R)Cl(PMe_3)_2 + NaNC_4H_2X_2 \rightarrow NiR(NC_4H_2X_2)(PMe_3)_2 + NaCl \quad (1)$$

a, X = H; **b**, X = Me

1, R = Me
2, R = CH_2SiMe_3
3, R = CH_2CMe_3
4, R = CH_2CMe_2Ph
5, R = 2,4,6-$C_6H_2Me_3$

that compounds **1–5** exist in solution[6] as square-planar species, with trans phosphine groups and a monohapto, N-bonded pyrrolyl ligand. They can therefore be considered as alkane- (or arene-) amide complexes of nickel.[7–10] Rather interestingly, **1b** forms

(1) Jolly, P. W.; Wilke, G. *The Organic Chemistry of Nickel*; Academic Press: New York, 1974.
(2) Jolly, P. W. *Comprehensive Organometallic Chemistry*; Wilkinson, G., Stone, F. G. A., Abel, E. W., Eds.; Pergamon Press: Oxford, England, 1982; Vols. 6 and 8.
(3) (a) Braunstein, P.; Matt, D.; Nobel, D. *Chem. Rev.* **1988**, *88*, 747. (b) Behr, A. *Angew. Chem., Int. Ed. Engl.* **1988**, *27*, 661.
(4) Yamamoto, T.; Kohara, T.; Yamamoto, A. *Bull. Chem. Soc. Jpn.* **1981**, *54*, 2161.
(5) Ibers, J. A. *Chem. Soc. Rev.* **1982**, *11*, 57.
(6) Solutions of compounds **1–5** are fairly stable to hydrolysis. This is at variance with the behavior found for $Ni(CH_2C_6H_4\text{-}o\text{-}Me)(NC_4H_2Me_2)(PMe_3)_2$, see: Carmona, E.; Marín, J. M.; Paneque, M.; Poveda, M. L. *Organometallics* **1987**, *6*, 1757.
(7) Chisholm, M. H. *Comprehensive Coordination Chemistry*; Wilkinson, G., Gillard, R. D., McCleverty, J. A., Eds.; Pergamon Press: Oxford, England, 1987; Vol. 2.

0020-1669/89/1328-1895$01.50/0